

Aggregation-Disruption-Induced Multi-Scale Mediating Strategy for Anticoagulation in Blood-Contacting Devices

Mingfei Pan, Zhaoyun Sun, Yuhao Zhang, Jiangwei Chen, Ziqian Zhao, Hongliang He, Hongbo Zeng,* Qingguo Li,* and Ning Gu*

Minimally invasive blood-contacting interventional devices are increasingly used to treat cardiovascular diseases. However, the risk of device-related thrombosis remains a significant concern, particularly the formation of cycling thrombi, which pose life-threatening risks. To better understand the interactions between these devices and blood, the initial stages of coagulation contact activation on extrinsic surfaces are investigated. Direct force measurements reveals that activated contact factors stimulate the intrinsic coagulation pathway and promote surface crosslinking of fibrin. Furthermore, fibrin aggregation is disrupted by surface-grafted inhibitors, as confirmed by ex vivo coagulation tests. An engineered serum protein with zwitterion grafts to resist the deposition of biological species such as fibrin, platelets, and red blood cells is also developed. Simultaneously, a protease inhibitor-based coacervate is incorporated into the coating to inhibit the intrinsic pathway effectively. The loaded coacervate can be released and reloaded through modulation of catechol-amine interactions, facilitating material regeneration. The strategy offers a novel multi-scale mediation strategy that simultaneously inhibits nanoscale coagulation factors and resists microscale thrombus aggregation, providing a long-term solution for anticoagulation in blood-contacting devices.

interventional operations.^[1] Among the most common interventions is the use of a central venous catheter, which introduces an operational probe transduced into the blood vessel to access the dysfunctional area. However, the insertion of extrinsic implants into the human body triggers a natural host response, stimulating the coagulation cascade, complement system, and immune response.^[2] Oral anticoagulation therapy is the most widely accepted protocol but carries bleeding risks and requires careful surveillance.^[3] Despite systemic anticoagulation, local thrombi on extrinsic materials frequently form, particularly in extracorporeal life support (ECLS) devices, posing risks for several postoperative complications, such as stroke, myocardial infarction, and pulmonary embolism. To address these challenges, developing a long-term anticoagulation strategy for hemocompatible cardiovascular implants is of high priority.

Thrombus formation on surfaces is a multi-scale process. At the nanoscale, the native circulatory system detects foreign

objects using soluble coagulation factor XII, known as the contact factor, which initiates the intrinsic coagulation cascade.^[4] This pathway sequentially upregulates the activities of factors XI/XIa, IX/IXa, X/Xa, and thrombin (II/IIa).^[5] Thrombin then

1. Introduction

The global rise in cardiovascular diseases has led to increased research into the human circulatory system and related

M. Pan, N. Gu
Key Laboratory for Bio-Electromagnetic Environment and Advanced Medical Theranostics
School of Biomedical Engineering and Informatics
Nanjing Medical University
Nanjing 211166, China
E-mail: guning@nju.edu.cn

M. Pan, Z. Zhao, H. Zeng
Department of Chemical and Materials Engineering
University of Alberta
Edmonton, Alberta T6G 1H9, Canada
E-mail: hongbo.zeng@ualberta.ca

Z. Sun, J. Chen, Q. Li
Cardiovascular Surgery
The Second Affiliated Hospital of Nanjing Medical University
Nanjing 210028, China
E-mail: liqg@njmu.edu.cn

Y. Zhang
School of Mechanical Engineering
Jiangsu Key Laboratory for Design and Manufacture of Micro-Nano Biomedical Instruments
Southeast University
Nanjing 211189, China

H. He
State Key Laboratory of Digital Medical Engineering
School of Biological Sciences & Medical Engineering
Southeast University
Nanjing 210009, China

N. Gu
Nanjing Key Laboratory for Cardiovascular Information and Health Engineering Medicine
Institute of Clinical Medicine
Medical School
Nanjing Drum Tower Hospital
Nanjing University
Nanjing 210093, China

The ORCID identification number(s) for the author(s) of this article can be found under <https://doi.org/10.1002/adma.202412701>

DOI: 10.1002/adma.202412701

converts soluble fibrinogen (FIB) into the insoluble fibrin network, which recruits cycling platelets. These platelets co-deposit, forming a microscale thrombus precursor. As red blood cells are subsequently recruited, the surface-deposited thrombus precursor grows into a macroscale thrombus, posing a risk for various vascular complications. Factor XII is also a specific immune cell regulator that promotes thromboinflammation by enzymatically converting plasma prekallikrein (PK) and high-molecular-weight kininogen (HMWK) into kallikrein (KLK) and bradykinin (BK), respectively.^[6] The inflammation is activated by BK and KLK, both part of the kallikrein-kinin system (KKS).

Current anticoagulation management for ECLS devices combines oral anticoagulants with surface anticoagulation coatings on circulation tubes, synergistically reducing both hemorrhagic and thrombotic events.^[7] Previous anticoagulation strategies for these devices mainly relied on inhibiting thrombin by activating antithrombin using heparin or its analogs.^[8] Another effective method involves the use of calcium chelates to deplete circulating calcium ions, thereby blocking the coagulation pathway.^[9] However, these bioactive methods inevitably result in complications including hemorrhage, hypertriglyceridemia, hyperkalemia, and even heparin-induced thrombocytopenia (HIT).^[10] Other commercially available methods include biopassive modification of the implant surface using superhydrophilic coatings or bovine serum albumin (BSA), which reduce the adsorption of plasma proteins.^[11] Additionally, slippery liquid-infused porous surfaces (SLIPS) inspired by *Nepenthes* pitcher plants demonstrate liquid-repelling properties that prevent the adhesion of fibrin/platelets and offer self-repairing properties for long-term anticoagulation.^[12] However, these current strategies lack active mediation of the initial thrombus formation event, particularly the contact activation of factor XII.^[13] Targeting XII-induced thromboinflammation has significant clinical significance with minimal influence on hemostasis.^[14] Developing an efficient surface anticoagulation strategy requires mediation on multiple scales, particularly during the initial event of contact activation.

In this study, we investigated the interactions between antibiofouling coatings and plasma proteins using surface force measurements in a confined space. The measurements were conducted using platelet-poor plasma (PPP), which preserves all coagulation factors and FIB. The coagulation cascade was activated by the injection of Ca^{2+} to enable the conversion of FIB to fibrin, stimulated by contact activation. The surface elastic modulus was then calculated using the Johnson–Kendall–Roberts (JKR) contact model to analyze thrombus skeleton formation.^[15] Based on the surface force measurements, we designed an innovative anticoagulation coating. Using a zwitterion sulfobetaine-grafted-BSA antibiofouling coating as the initial layer, we designed a catechol-amine-derived coacervate, encapsulating two small molecules on the top: gallic acid (GA) and the tryptase inhibitor FUT-175 (Figure 1A).^[16] The tryptase inhibitor FUT-175 has been registered and approved in Japan and Korea for the treatment of disseminated intravascular coagulation, with a lower risk of bleeding.^[17] The GA/FUT-175 (GA/F) coacervate was served as the second layer and deposited on the initial layer by tuning the catechol chemistry under physiological salinity conditions.^[18] The enrichment of these intrinsic coagulation inhibitors from the solution to the coating surface facilitates contact inhibition of XII, whereas the zwitterion grafts disrupt the deposition of

macromolecules in the blood, including platelets (PLTs), fibrin networks, and red blood cells (RBCs) (Figure 1B). The precise design of these surface functionalities suggests that this bifunctional coating mediates the coagulation cascade from nanosized coagulation factors to micro-sized thrombus skeletons, demonstrating the potential of our multi-scale mediating strategy (transdimension inhibition from nanoscale to microscale) shows significant potential for use in cardiovascular implants, improving biosafety in interventional medicine (Figure 1C).

2. Results and Discussion

We developed an anticoagulation coating using a two-step deposition strategy with zwitterion sulfobetaine-grafted BSA as the coating skeleton and a GA/FUT-175-derived coacervate as the surface-anchored inhibitor of the intrinsic coagulation pathway. Following our previous procedure, the BSA molecules (15 mg mL^{-1} , pH 6.5) were first reduced using tris(2-carboxyethyl)phosphine (TCEP, 10 mg mL^{-1}) to generate free thiols ($-\text{SH}$). These thiols reacted with the carbon-carbon bonds of sulfobetaine methacrylate monomer via Michael addition under 365 nm UV irradiation, inducing continuous polymerization for over 24 h.^[16] During polymerization, GA-NHS ester (1 mg mL^{-1}) was added to the sulfobetaine (SBA)–BSA solution to react with the free amine groups of BSA and introduce polyphenolic groups as active sites for further modification. The resulting SBA-grafted (B/SBA) and SBA/GA-grafted (B/SBg) were dialyzed and freeze-dried. Conformational changes in BSA during the bi-grafting process were characterized by circular dichroism (Figure 2A) and UV–vis spectroscopy (Figure S1A, Supporting Information). The decrease in α -helix peaks at 208 and 222 nm, along with the reduction in hydrodynamic radius (Figure S2, Supporting Information) from BSA to B/SBA, indicates a conformational change after the reduction with TCEP. However, the lesser variation in chirality from B/SBg to BSA suggests that grafted polyphenol maintains the α -helix structure of BSA through hydrogen bonding.^[19] The reduced BSA generated amyloid-like protein aggregates, creating a durable substrate deposition with great durability in harsh environments, which benefits the application of ECLS in this study.^[19,20] The second layer of the coating was derived from the two small molecules of GA and FUT-175. The corresponding mechanism was first investigated using isothermal titration calorimetry (ITC), where FUT-175 was titrated into GA at pH 5.5 and 7.5 (Figure 2B; Figure S3, Supporting Information). The raw output of the ITC experiment for the heat exchange rate per injection at pH 5.5 and 7.5 was calculated to obtain the heat of injection as a function of the molar ratio (Figure 2C). The green line shows the fitted results of titration at pH 5.5 with no apparent enthalpy change ($\Delta H = 0 \text{ kJ mol}^{-1}$) while the red line corresponding to the titration at pH 7.5 is a significant exothermic process with ΔH , ΔS , and ΔG values of -48.27 , -72.98 , and $-25.63 \text{ kJ mol}^{-1}$, respectively. Meanwhile, a relatively strong absorption from UV–vis spectra of GA/F (pH 7.5) $\approx 370 \text{ nm}$ associated with the formation of $\text{C} = \text{C} = \text{N}$ and $\text{C} = \text{C} = \text{O}$ compared to that of GA/F (pH 5.5), shown in Figure S1B (Supporting Information). These results are consistent with the ΔG of GA/F interaction from ITC data in an alkaline environment.^[21] The higher ΔG and corresponding UV peaks suggest the strong interactions between FUT-175 and GA under the alkaline environment which

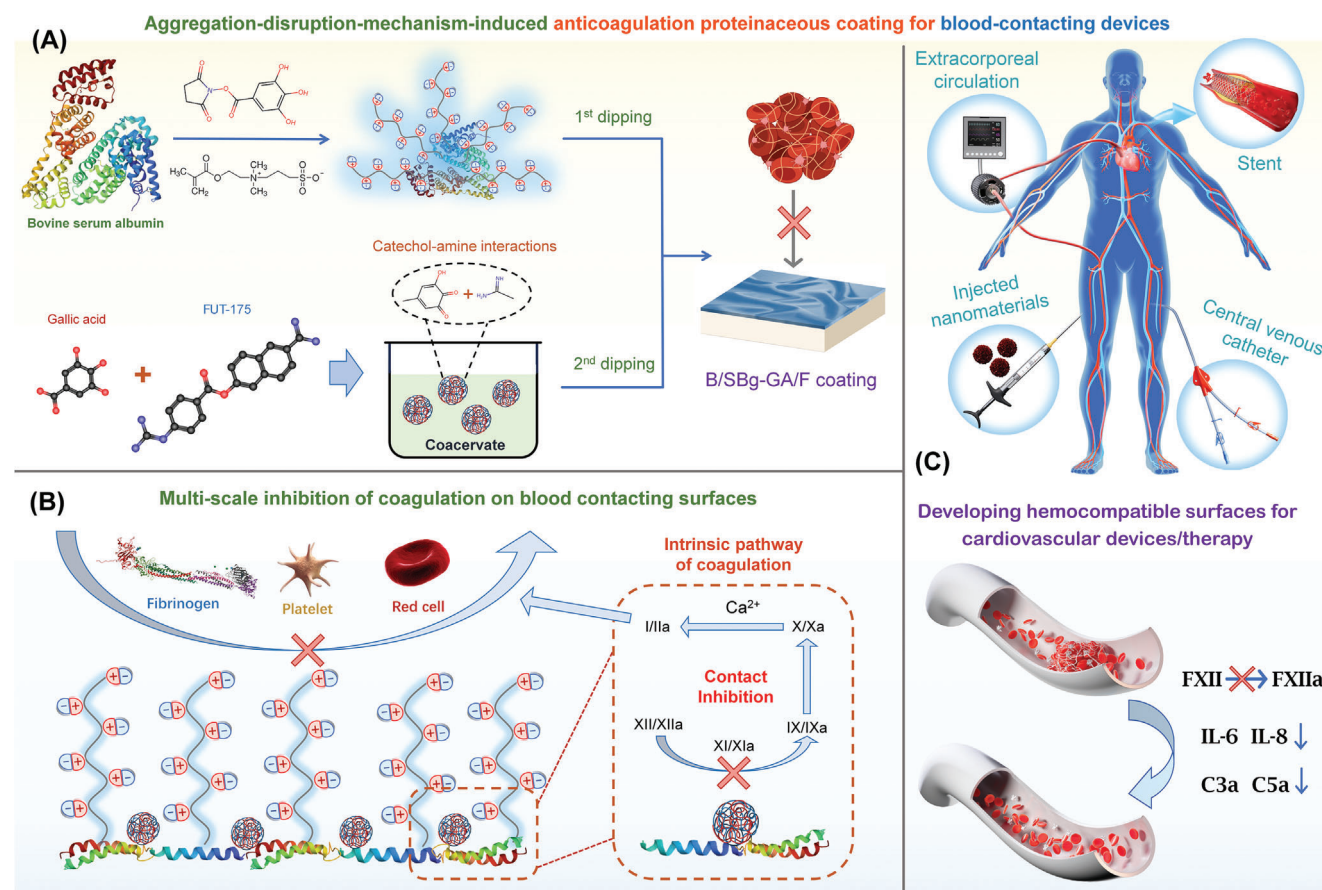


Figure 1. A) Design of an anticoagulation proteinaceous coating with zwitterion-grafted BSA as the bottom layer and GA/F pharmacological coacervate as the top layer; B) Multi-scale inhibition of coagulation on blood-contacting surfaces by inhibiting the activation of nanoscale coagulation factors and resisting the deposition of microscale fibrin networks, PLTs, and RBCs; C) Schematic of the potential clinical application of the developed coating, illustrating its molecular mechanisms for mediating thromboinflammation by inhibiting the activation of the intrinsic coagulation pathway, immune response, and complement system.

is consistent with the reaction kinetics of the Michael addition and Schiff-base interactions of catechol chemistry.^[22] Additionally, the zeta potentials of the developed GA/F were significantly higher than those of B/SBg from pH 5–8 (Figure S4, Supporting Information), which can be ascribed to the positively charged guanidine moieties in the GA/F coacervates. The as-prepared GA/F copolymer, which underwent phase separation (molar ratio of 3:1), was deposited on the B/SBg coating using polyphenol-amine interlinks and electrostatic interactions.

The chemical functionality of the coating was identified using Fourier transform infrared (FTIR) and X-ray photoelectron spectroscopy (XPS). Characteristic peaks at 1648, 1542, and 1234 cm^{-1} correspond to amides I, II, and III from the BSA moieties, while peaks at 1037 and 780 cm^{-1} correspond to the S = O stretching of SBg and –NH– wagging, respectively.^[23] Shifts in the amide III may correlate with the grafting of GA via amide bonds, whereas the enhanced intensity of –NH– wagging peaks is linked to the guanidino groups of FUT-175.^[24] The XPS characteristic peaks for –N⁺ and –SO³⁻ also indicate the effective conjugation of SBg to BSA (Figure 2E; Figure S5, Supporting Information).^[25] Specifically, the appearance of the XPS characteristic peaks for –N=C was associated with the coat-

ing of GA/F, confirming the formation of a Schiff base reaction for interconnecting GA/F to B/SBg.^[26] Surface wettability and topography of the developed coatings on PVC substrates were characterized by water contact angle (WCA) measurements in air and field-emission scanning electron microscopy (SEM) with energy-dispersive X-ray spectroscopy (EDS). The WCA of the bare polyvinyl chloride (PVC) film was $\approx 85^\circ$, which decreased to 54° upon the introduction of BSA, and further reduced to 45° with the addition of B/SBg on the PVC film, suggesting enhanced hydrophilicity due to zwitterion grafting (Figure 2F). The coating morphology (Figure 2G; Figure S6, Supporting Information) with continuous modification of B/SBg on PVC tubes and secondary modification of GA/F spheres (diameter in the dry state ≈ 150 nm, hydrodynamic diameter ≈ 282 nm) uniformly embedded on top of B/SBg. These physical and chemical characterizations demonstrated the successful synthesis and deposition of B/SBg-GA/F coatings on PVC substrates.

The initial stages of the coagulation process on extrinsic surfaces were investigated using surface forces apparatus (SFA) with the effect of surface functionalities. Surface force measurements were conducted in diluted platelet-poor plasma (PPP, diluted 20 times) containing all coagulation factors and FIB (Figure 3A).

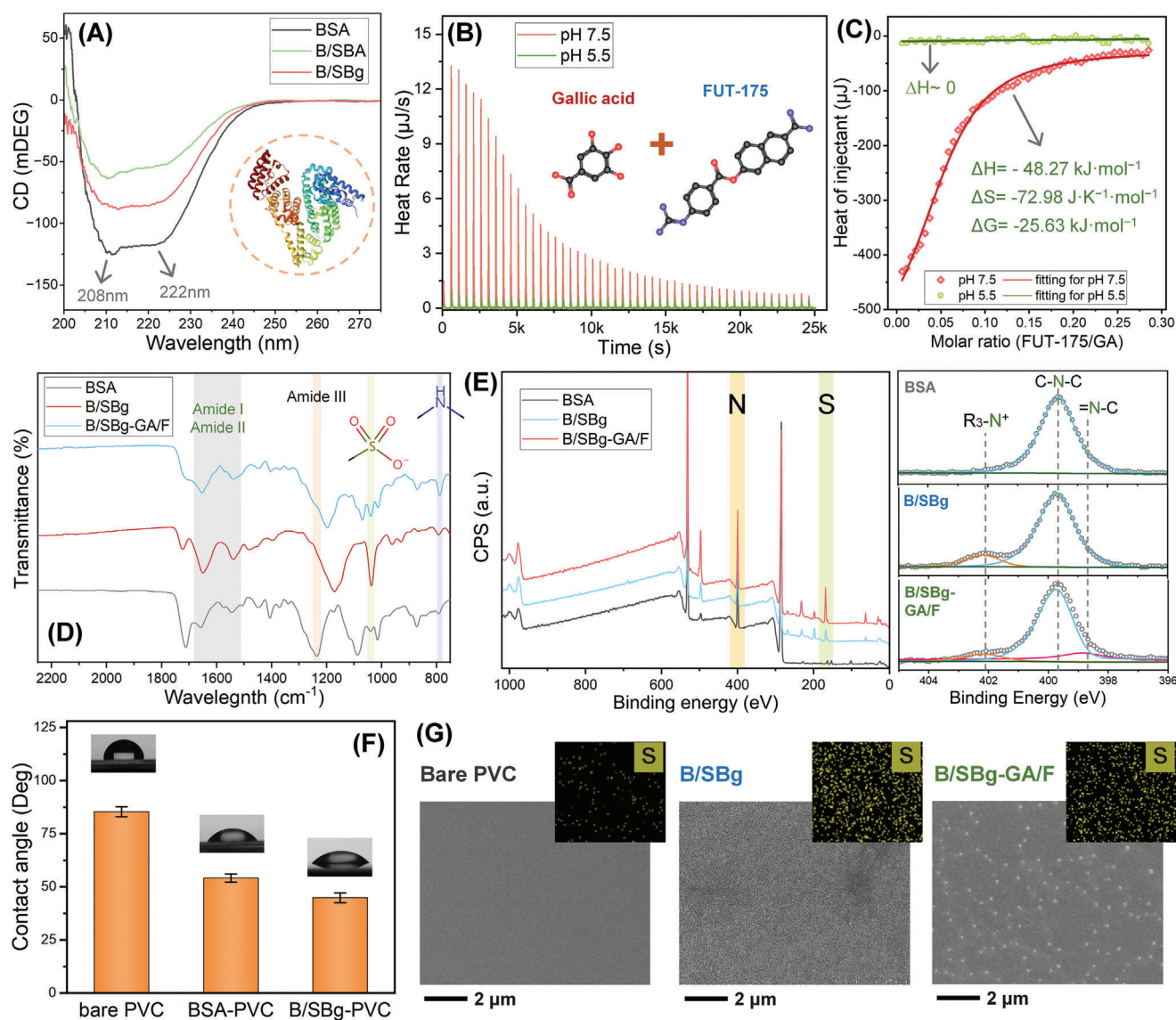


Figure 2. A) Circular dichroism spectra of the developed materials; B) Isothermal titration calorimetry characterization of the reactions between GA and FUT-175 at different pH with C) corresponding model fitting; D) FTIR spectra of BSA, B/SBg, and B/SBg-GA/F coating on PVC wafers; E) XPS wide scan spectra of BSA, B/SBg, and B/SBg-GA/F coating on PVC wafers with high-resolution N deconvolution spectra; F) Water contact angle in air measurement on bare, B/SBg-, and B/SBg-GA/F-coated PVC wafers; G) SEM images of bare, B/SBg-, and B/SBg-GA/F-coated PVC wafers with EDS mapping (inset) at the same frame with a magnification of 10 k.

The use of PPP excludes the undesirable steric repulsion from platelets and blood cells.^[27] The mica surface was functionalized with B/SBg and B/SBg-GA/F coatings, and the coating thickness was first characterized in PBS (Figure 3B). The measurements were conducted in citrated PPP (c-PPP), where the coagulation pathway was inhibited by the depletion of Ca²⁺. The plasma protein deposition thickness (ΔD) is calculated to be ≈ 9 and 11 nm on B/SBg and B/SBg-GA/F coating, respectively, compared to $\Delta D \approx 50 \text{ nm}$ on the uncoated mica surface. This reduction in plasma protein deposition was ascribed to the grafting of zwitterionic moieties onto the BSA. The dense hydration layer generated by zwitterionic grafts on a proteaceous framework has been previously shown to provide superior resis-

tance to biofouling, even under harsh environments.^[28] Upon adding Ca²⁺ to initiate the intrinsic coagulation pathway, ΔD increased significantly in all cases, with minimal hardwall separation. This phenomenon is associated with a reduction in FIB activated by XIIa, which eventually induces the formation and surface deposition of an elastic fibrin network. The protein deposition thickness is summarized in Figure S7 (Supporting Information), and the corresponding surface elastic modulus was calculated using the JKR contact model (Figure 3C). The elastic modulus of mica increased from 428 kPa in c-PPP to 980 kPa in PPP. Meanwhile, the elastic modulus of B/SBg decreased from 1770 kPa in c-PPP to 533 kPa in PPP, suggesting the formation of a looser fibrin network on the zwitterion-grafted

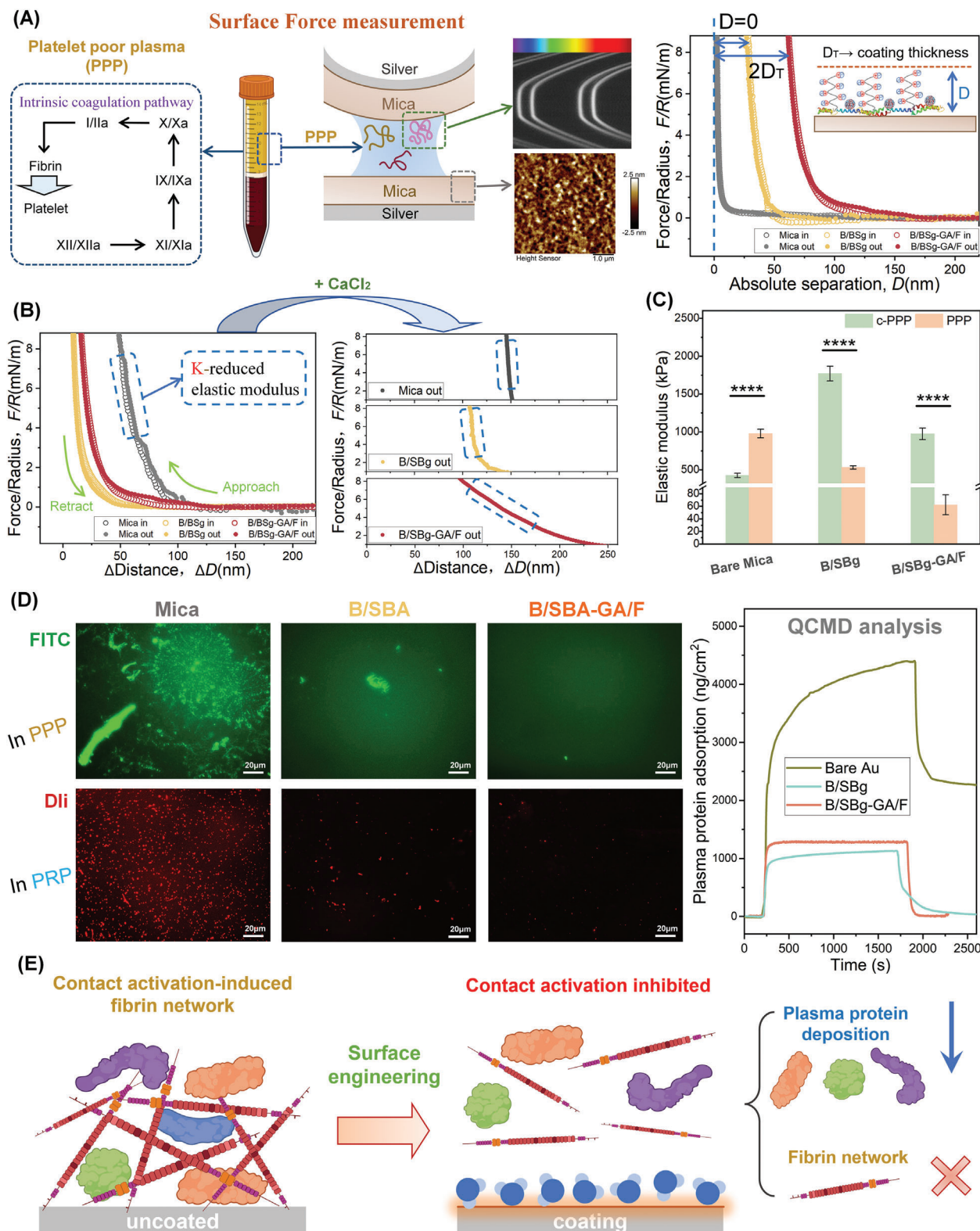


Figure 3. Nanomechanics of anticoagulation coatings. A) Schematic of SFA force measurement in PPP and force-separation profiles of coatings on mica in PBS; B) Force-separation profiles of coatings on mica in c-PPP and PPP with C) corresponding elastic modulus (\pm SD for $n = 3$ replicates per condition, $p < 0.0001$); D) Fluorescence microscopy images (gain = 650%, exposure time = 450 ms) showing protein disposition and platelet adhesion on different substrates with the QCMD tests monitoring dynamic surface plasma adsorption in PPP; E) Proposed mechanisms of the developed coating reducing the plasma protein deposition and disrupting fibrin network formation.

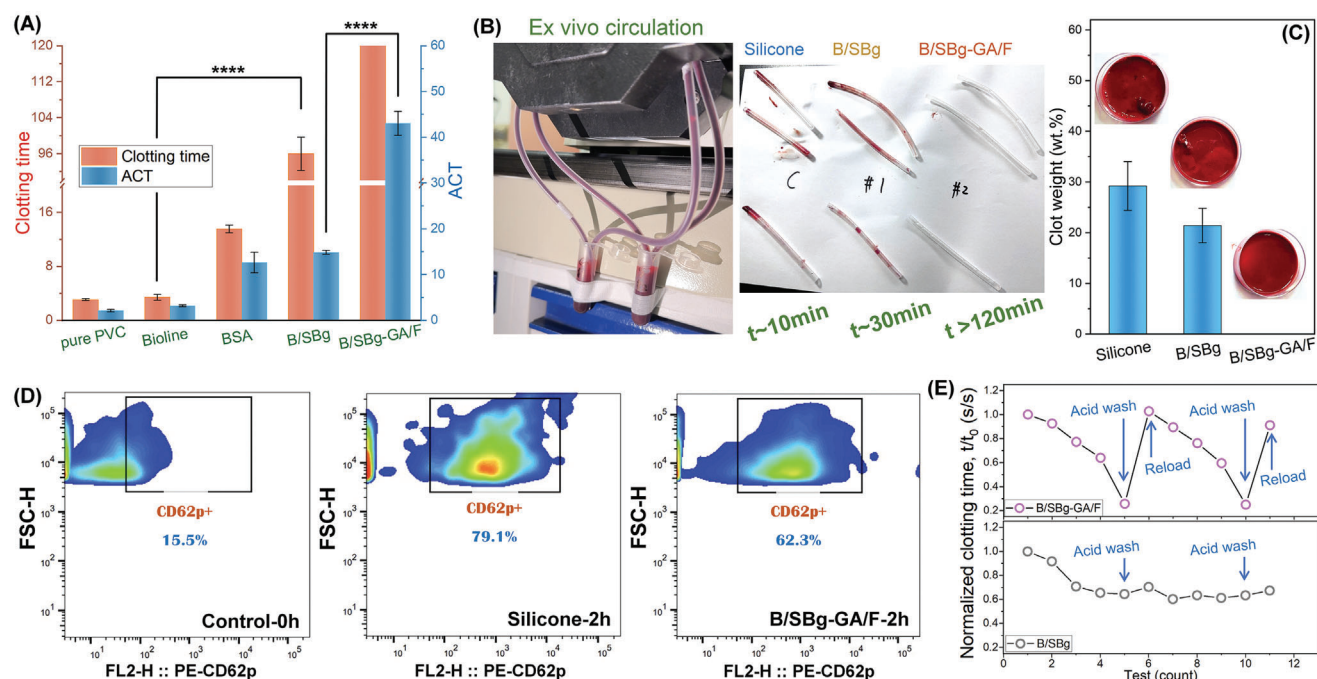


Figure 4. Anticoagulation performance. A) CT and ACT of bare, Bioline, BSA-coated, B/SBg-coated, and B/SBg-GA/F-coated PVC tubes (\pm SD for $n = 3$ replicates per condition, $p < 0.0001$); B) Optical images showing ex vivo circulation with the tubes and C) clot weight ratio in blood after the experiment; D) Scatterplot of CD62p⁺ measured from the blood after 2 h extracorporeal circulation using bare and B/SBg-GA/F-coated silicone tubes (represent the level of the activated platelet) with fresh blood as the control group at 0 h; E) Normalized clotting time with the cycling tests on the surface of B/SBg and B/SBg-GA/F-coated PVC tubes.

BSA. The elastic modulus of the B/SBg-GA/F coating further reduced from ≈ 975 kPa for c-PPP to 62 kPa for PPP, suggesting that GA/F effectively interfered with the coagulation-induced aggregation under contact activation through the pharmacological activity of FUT-175 targeting XII and XI. The surface aggregation state of fibrin in PPP was confirmed by the observation using the fluorescein isothiocyanate (FITC) staining and the recruitment of DiI-labeled platelets in platelet-rich plasma (PRP) (Figure 3D). The dynamic adsorption of plasma proteins on the developed coatings was monitored using a quartz crystal microbalance with dissipation (QCM-D, Figure 3D; Figure S7C, Supporting Information), which demonstrated a relatively low amount of protein adsorption under flow conditions. These force measurements and characterizations demonstrate that the B/SBg and GA/F moieties of the developed coating synergistically intermediate the initial coagulation process on blood contact surfaces, by resisting plasma protein attachment non-specifically and by specifically inhibiting the intrinsic coagulation pathway.

The anticoagulation performance of the developed coatings was characterized using ex vivo tests. The criteria for selecting the FUT-175 concentration during the PVC tube-coating process were investigated using the activated clotting time (ACT, activating XII), as summarized in Figure S8 (Supporting Information). The measured ACT increased significantly with FUT-175 concentration in the coating solution from 0 to 3 mg mL⁻¹, whereas the ACT was less concentration-sensitive for FUT-175 concentrations greater than 3 mg mL⁻¹. Hence, the GA/F (1.5/3 mg mL⁻¹) pharmacological coacervate was employed for deposition on the target substrates. Figure 4A shows clotting time (CT) and ACT

measurements of fresh rat arterial blood in contact with different substrates (Figure S9, Supporting Information). Compared to bare PVC tubes, the CT and ACT of the B/SBg-coated PVC tubes increased by $\approx 3010\%$ and 550% , respectively. The CT and ACT for B/SBg coatings were also significantly higher than those of pristine BSA coating, implying a shielding effect of the zwitterionic B/SBg coating. The CT and ACT of B/SBg were further prolonged to over 140 and 43 min, respectively, showing a 4100% and 2000% increase compared to bare PVC. Meanwhile, the anticoagulation performance of B/SBg was substantially greater than that of commercial Bioline anticoagulation tubes (heparin-coated), showing 3700% and 1200% enhancements in CT and ACT, respectively. Based on the excellent performance observed in the static clotting time tests, we conducted ex vivo circulation using fresh rat arterial blood (Figure 4B). The condition of the silicone tubing and blood after circulation is shown in Figure 4B,C, respectively. The groups for bare and B/SBg-coated silicone tubing were clogged after ≈ 10 and 30 min, respectively, which is consistent with the results of the static clotting time, indicating that B/SBg delayed the occurrence of clotting, but provided limited coagulation inhibition. However, circulation of B/SBg-GA/F lasted for more than 2 h. The clot weight fraction is illustrated in Figure 4C, with no adherent clots observed on the circulation tubes with the B/SBg-GA/F coating after PBS washing. The antifouling phenomenon of the B/SBg-GA/F coating is consistent with QCM-D tests, indicating that both the zwitterionic moieties and GA/F coacervates inhibited thrombus formation and adhesion. After 5 min of circulation, blood samples were collected for coagulation parameters, including

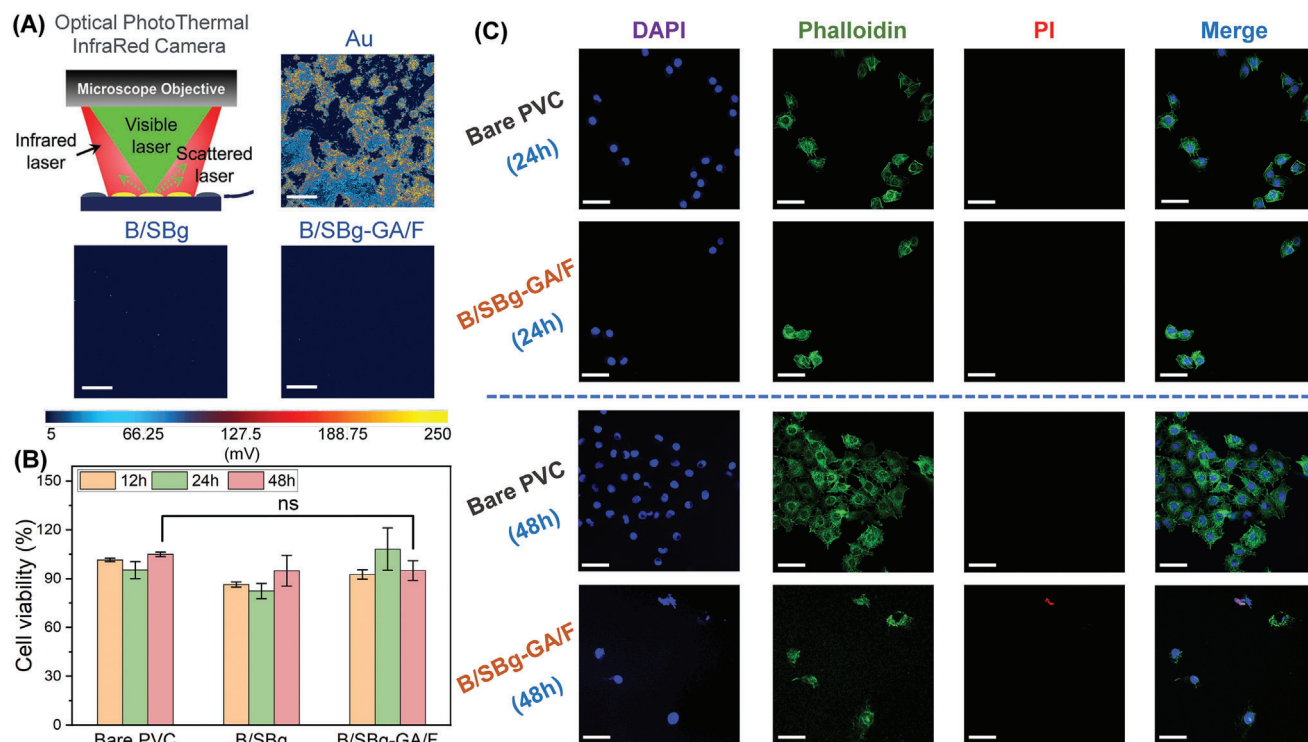


Figure 5. Biocompatibility tests. A) Optical photothermal infrared (O-PTIR) mappings of bare, B/SBg-coated, and B/SBg-GA/F-coated Au wafer after immersion in whole blood (scanned at 1650 cm^{-1}); B) Viability of HUVEC cells after 12, 24, and 48 h of incubation with bare, B/SBg-coated, and B/SBg-GA/F-coated PVC wafer (\pm SD for $n \geq 3$ replicates per condition, $p > 0.05$), evaluated by CCK-8 assay; C) Fluorescence microscopy images (gain = 500%, exposure time = 320 ms) showing cell nuclei and actin filaments on bare and B/SBg-GA/F-coated wafer surfaces after 48 h of incubation (scale bar, $40\text{ }\mu\text{m}$).

prothrombin time (PT), thrombin time (TT), activated partial thromboplastin time (APTT), and FIB level (Figure S10, Supporting Information). Compared to fresh blood samples, the decreases in PT, TT, APTT, and FIB of the blood samples with bare tubes indicate activation of factor XII/thrombin and fibrin formation. In contrast, increases in APTT of the blood samples with the B/SBg-GA/F-coated tubes indicate an inhibited intrinsic pathway with minimum influence on the extrinsic pathway and FIB. The stability of the coating was investigated through circulation tests under different shear forces using PBS as the washing solution (Figure S11, Supporting Information). The B/SBg-GA/F coating exhibited a certain degree of resistance to shear rate up to $106\text{--}637\text{ s}^{-1}$ while ACT decreased significantly at shear rates of 955 and 1274 s^{-1} . However, the anticoagulation property (ACT measurement) of the B/SBg-GA/F-coated tubes under high shear rates washing at 1274 s^{-1} was still $\approx 30\%$ higher than that of commercial Bioline anticoagulation tubes. Release studies of B/SBg-GA/F from the tube surfaces into the blood were further characterized (Figures S12 and S13, Supporting Information). The dose of the released B/SBg-GA/F is within the range of $5\text{--}50\text{ }\mu\text{g mL}^{-1}$ at shear rates from 106 to 1274 s^{-1} compared to the therapeutic dose of FUT-175 ($\approx 300\text{ }\mu\text{g mL}^{-1}$ blood concentration), suggesting the robustness of B/SBg-GA/F under clinical settings. CD62p, a type-1 transmembrane protein involved in platelet membrane procoagulation adhesion, was selected as a biomarker in this study.^[29] The activation of the platelet (CD62p^+ , “+” represents the activated state) after the circulation is deter-

mined by flow cytometry, with the fresh artery blood at 0 h as the control group. Compared to bare PVC tubes, the B/SBg-GA/F-coated tubes decreased CD62p expression by 16.8% , suggesting that fewer platelets were activated after extracorporeal circulation, followed by a reduction in the potential recruitment of red blood cells to generate thrombi. Due to the controllable association/dissociation nature of catechol-amine interactions, the GA/F coacervates could undergo a loading/reloading process on the B/SBg coatings to regenerate their anticoagulation capability. Figure 4E shows the variation in clotting time during cycling tests (depletion of FUT-175 inhibitors) and the recovery of the anticoagulation effect after acid washing (disassociation of catechol-amine interactions) and GA/F reloading in an alkaline environment.^[30] The tunable surface functionality of GA/F endows the B/SBg-GA/F coating with versatility, enhancing its potential for clinical translation.

Given the significant anticoagulation performance of the B/SBg-GA/F coating observed in ex vivo tests, its biocompatibility was investigated using 2D infrared imaging and cell culture assays. After immersion in blood for 4 h and washing with DI water, the protein residues were characterized using photothermal infrared (OPTIR) microscopy. OPTIR is a noncontact technique that couples visible and infrared lasers to precisely image surface chemical information based on their characteristic IR peaks. Figure 5A shows IR images of bare, B/SBg-coated, and B/SBg-GA/F-coated Au surfaces at the amide A peak (wavelength of 1650 cm^{-1} corresponding to plasma proteins, Figure S14,

Supporting Information). Compared with the bare Au surface, the coverage of the deposited protein on both the B/SBg- and B/SBg-GA/F-coated Au surfaces was significantly reduced, with only trace signals detected. The fouling resistance capability of the developed coating prevented the formation of undesirable biofilms on implants. Figure 5B shows the cell viability of the bare, B/SBg-coated, and B/SBg-GA/F-coated PVC substrates using HUVEC, with no significant cell toxicity observed within 48 h of incubation. Fluorescence microscopy was employed to further investigate the interaction of cells with the developed coatings, visualizing the morphology of 2D cell growth by dyeing the nuclei with 4',6-diamidino-2-phenylindol (DAPI) and propidium iodide (PI), the actin filaments with Phalloidin. As shown in Figure 4C, the cells maintained an intact actin filament with no apparent membrane destruction (PI staining) over the 24–48 h period. These results indicate the excellent antifouling properties and biocompatibility of the developed B/SBg-GA/F coating, making it highly suitable for use in implantable materials.

To further investigate the anticoagulation mechanisms of the B/SBg-GA/F coating, femoral vein-to-auricular artery (V-A) intubation (Figure 6A) was conducted in rabbits to establish extracorporeal circulation. Figure 6B shows the arterial blood test results after intubation, with the flow rate set to 30 mL min⁻¹ (shear rate of ≈ 637 s⁻¹), which is equivalent to a moderate shear rate in clinical ECLS.^[31] The blood tests indicated successful intubation in rabbits with steady physiological indices, through a decrease in PLTs/RBCs and an increase in white blood cells (WBCs) were also observed after incubation to bare silicone circulation tubes. This could be attributed to the occurrence of thromboinflammation, which induces the depletion of PLTs/RBCs to generate thrombi and inflammation-derived WBC elevation. Figure 6B shows the secretion of BK, KLK, von Willebrand Factor (vWF), complement components C3a and C5a, interleukin-6 (IL-6), and interleukin-8 (IL-8) measured in the serum from arterial blood after V-A intubation. The increase in BK and KLK expression with bare tubes at 4 h compared to that at 0 h implies contact activation of XII, which enzymatically converts PK/HMWK into KLK/BK, whereas BK and KLK expression with B/SBg-GA/F-coated tubes at 4 h was downregulated compared to that with the bare tubes at 4 h, suggesting the suppression of contact activation of the intrinsic coagulation pathway (XII). The vWF is associated with the protection of factor VIII, which belongs to the intrinsic pathway, and platelet adhesion. Upregulation of vWF correlates with clinical thrombotic events.^[32] The level of vWF expression in the B/SBg-GA/F-coated tubes was 53.2% lower than that in the bare tubes, indicating inhibition of coagulation with the developed coating. The complement system is activated by blood interactions with extrinsic material surfaces that are associated with the activation of innate immunity and proinflammatory pathways. The levels of the complements C3a and C5a with the B/SBg-GA/F-coated tubes were significantly lower than those with the bare tubes, likely due to the absorption resistance of the coatings to the complements C3a and C5a. A similar trend was observed for the secretion of IL-6 and IL-8, suggesting an inhibited immune response in the B/SBg-GA/F. To simulate the use of extracorporeal circulation in clinical scenarios, the rabbit model that is vein-injected with prophylactic dose (0.5 mg kg⁻¹ per 8 h) of low molecular weight heparin was used for long-term V-A intubation up to 12 h. The results of the blood tests and thromboin-

flammation after intubation are illustrated in Figure S15 (Supporting Information), demonstrating that the B/SBg-GA/F coating effectively reduced tube-related thrombosis coupled with low doses of heparin during extracorporeal circulation. In summary, the B/SBg-GA/F coating developed in this study exhibits significant potential to reduce material-related thromboinflammation by inhibiting contact activation and preventing adsorption-induced complement system activation. The clinical use of FUT-175 in systemic anticoagulation therapy is limited by its short half-life of ≈ 8 min. The assembly of FUT-175 in the GA/F coacervate for localized anticoagulation prolongs its functional duration (>12 h), offering a promising pharmaceutical coating solution for ECLS.

For blood-contacting surfaces, the inflammatory response triggered by material-blood interactions, which leads to tissue and cell alteration, exudation, proliferation, and aggregation of inflammatory cells, is crucial for long-term biosafety. Figure S16 (Supporting Information) and Figure 6C illustrate the hematoxylin and eosin (H&E) and immunohistochemistry (IHC) staining of the mouse lung, liver, kidney, and heart after 48 h of exposure to B/SBg-GA/F. Histologically, no alterations, exudation, proliferation, or infiltration of inflammatory cells such as lymphocytes, plasma cells, eosinophils, or neutrophils into the interstitium were observed. Meanwhile, no significant change in the immunohistochemical expression of the CD-45 molecular marker was observed within 48 h, suggesting that the heart, liver, kidney, and lungs secreted limited inflammation-related proteins in response to the foreign object of B/SBg-GA/F. In addition, B/SBg-GA/F was functionalized on a thermocouple to monitor blood temperature contact (Figure S17A, Supporting Information). The coagulation pathway was activated by adding Ca²⁺ at the time point of 0 min. The B/SBg-GA/F-coated sensor exhibited a faster response rate to temperature variations compared to the B/SBg-coated stainless steel sensor after 20 min of measurement (Figure 6D; Figure S17B, Supporting Information). This difference may be attributed to thrombus formation on the B/SBg-coated sensor (observed from the optical images), which interfered with heat conduction. The pharmacological action of B/SBg-GA/F actively inhibits thrombus formation on the temperature sensors, suggesting that it can be applied to various blood-contacting sensors and devices that require a pristine surface for optimal performance.

3. Conclusion

In conclusion, we have demonstrated an innovative anticoagulation strategy combining proteaceous B/SBg with GA/FUT-175 pharmacological coacervates. The B/SBg coating, with its zwitterionic moieties, demonstrated robust resistance to biomacromolecule adhesion, whereas the GA/FUT-175 coacervates inhibited initial contact activation and the intrinsic coagulation pathway. Compared to commercial bioline anticoagulation tubes, our approach resulted in significant increases in CT and ACT by 3700% and 1200%, respectively. The superior anticoagulation performance originated from a reduced thromboinflammatory response, as evidenced by changes in aggregation states from nanosized coagulation factors to micro-sized fibrin networks, platelets, and RBCs, as comprehensively investigated using SFA. The coating effectively inhibited the intrinsic coagulation

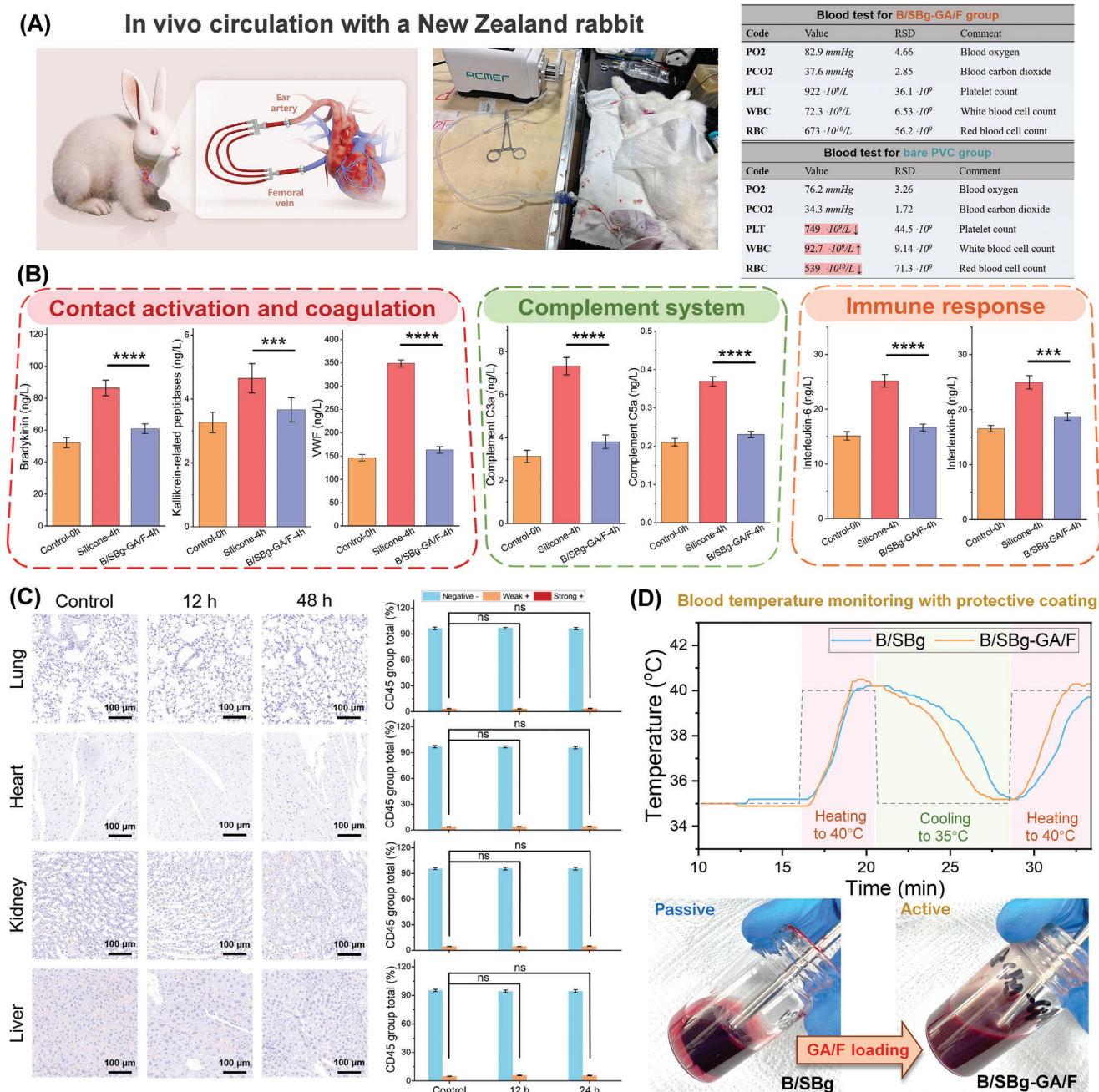


Figure 6. A) Femoral vein to ear artery to (V-A) extracorporeal circulation in rabbits with blood tests after 4 h of intubation (RSD for root square deviation, $n \geq 3$ replicates per condition); B) Secretion of contact activation-related BK, KLK, coagulation-related vWF factor, complement system-related C3a, C5a, and immune-related IL-6, IL-8 measured with bare and B/SBg-GA/F-coated tubes after 4 h of intubation (\pm SD for $n \geq 3$ replicates per condition, $p < 0.001$); C) CD-45 immunohistochemistry (IHC) staining images of the lung, liver, kidney, and heart of mice injected with B/SBg-GA/F at 0, 12, and 24 h (\pm SD for $n = 3$ replicates per condition, $p > 0.05$); D) Temperature measurement with B/SBg and B/SBg-GA/F-coated thermocouple under varying environmental temperatures with photos showing blood status after 40 min of measurement.

pathway, complement system activation, and inflammation, as confirmed by enzyme-linked immunosorbent assays. This study not only demonstrates an energetic paradigm for converting accessible biomacromolecules into versatile proteaceous coatings but also provides a novel approach for inhibiting host response-induced thromboinflammation via a multiscale mediating strategy. These findings hold significant potential for a wide range

of interventional biomedical applications involving implantable materials.

4. Experimental Section

Animal Ethics Statement: The blood sample collection and animal procedures conformed to the legal requirements in China and were approved

by the Animal Ethics Committee of Nanjing Medical University (No.s 14730–2201043, 15148–2206032).

Statistical Analysis: Averaged values and standard deviation SD are calculated from at least three different measurements for each entry. The data were processed by Excel (version 2405) and classified according to the p values (t-test, two-sided) and denoted by (ns) for $p > 0.05$, (*) for $p > 0.05$, (**) for $p > 0.01$, (***) for $p > 0.001$, and (****) for $p > 0.0001$.

Chemicals, materials, and methods are available in the supporting information.

Supporting Information

Supporting Information is available from the Wiley Online Library or from the author.

Acknowledgements

M.P. and Z.S. contributed equally to this work. The authors are grateful for the financial support from the Natural Sciences and Engineering Research Council of Canada (NSERC), Canada Research Chairs Program (H. Zeng), the National Natural Science Innovative Research Group Project (No. 61821002), National Natural Science Foundation of China (No. 32401084), the Frontier Fundamental Research Program of Jiangsu Province for Leading Technology (No. BK20222002), Medical-Industrial Integration Project of the Second Affiliated Hospital of Nanjing Medical University (No. YGRH005).

Conflict of Interest

The authors declare no conflict of interest.

Data Availability Statement

The data that support the findings of this study are available from the corresponding author upon reasonable request.

Keywords

anticoagulation, blood-contacting devices, intrinsic pathway, multi-scale biomechanics

Received: August 26, 2024

Revised: September 11, 2024

Published online: September 30, 2024

- [1] a) N. Ijaz, B. Buta, Q.-L. Xue, D. T. Mohess, A. Bushan, H. Tran, W. Batchelor, C. R. DeFilippi, J. D. Walston, K. Bandeen-Roche, *J. Am. Coll. Cardiol.* **2022**, 79, 482; b) J. A. Leopold, J. Loscalzo, *Circ. Res.* **2018**, 122, 1302; c) M. Kivimäki, A. Steptoe, *Nat. Rev. Cardiol.* **2018**, 15, 215.
- [2] a) I. H. Jaffer, J. I. Weitz, *Acta Biomater.* **2019**, 94, 2; b) J. L. Brash, T. A. Horbett, R. A. Latour, P. Tengvall, *Acta Biomater.* **2019**, 94, 11.
- [3] a) G. Annich, *J. Thromb. Haemost.* **2015**, 13, S336; b) M. Mazzeffi, J. Greenwood, K. Tanaka, J. Menaker, R. Rector, D. Herr, Z. Kon, J. Lee, B. Griffith, K. Rajagopal, *Ann. Thoracic Surg.* **2016**, 101, 682.
- [4] a) N. Naito, R. Ukita, J. Wilbs, K. Wu, X. Lin, N. M. Carleton, K. Roberts, S. Jiang, C. Heinis, K. E. Cook, *Biomaterials* **2021**, 272, 120778; b) J. Xu, Y. Zhang, J. Xu, G. Liu, C. Di, X. Zhao, X. Li, Y. Li, N. Pang, C. Yang, *Adv. Mater.* **2020**, 32, 1905145.
- [5] D. A. Hickman, C. L. Pawlowski, U. D. Sekhon, J. Marks, A. S. Gupta, *Adv. Mater.* **2018**, 30, 1700859.
- [6] a) A. Schmaier, *J. Thromb. Haemost.* **2016**, 14, 28; b) H. He, Q. Han, S. Wang, M. Long, M. Zhang, Y. Li, Y. Zhang, N. Gu, *ACS Nano* **2023**, 17, 14555; c) F. Yang, G. Guo, Y. Wang, *Biomaterials* **2022**, 289, 121761.
- [7] C. Vandenbriele, D. J. Arachchilage, P. Frederiks, G. Giustino, D. A. Gorog, M. Gramegna, S. Janssens, B. Meyns, A. Polzin, M. Scandroglio, *J. Am. Coll. Cardiol.* **2022**, 79, 1949.
- [8] S. J. Paluck, T. H. Nguyen, H. D. Maynard, *Biomacromolecules* **2016**, 17, 3417.
- [9] T. Xu, H. Ji, L. Xu, S. Cheng, X. Liu, Y. Li, R. Zhong, W. Zhao, J. N. Kizhakkedathu, C. Zhao, *Nat. Commun.* **2023**, 14, 4875.
- [10] a) S. E. Claudel, L. A. Miles, M. Murea, *Seminars in Dialysis* **2021**, 34, 103; b) A. Greinacher, *N. Engl. J. Med.* **2015**, 373, 252.
- [11] Z. Sun, X. Guan, M. Pan, J. Chen, L. Ding, T. He, X. Wang, K. Xu, Z. Cui, W. Tong, *Prog. Org. Coat.* **2024**, 190, 108368.
- [12] a) T.-S. Wong, S. H. Kang, S. K. Tang, E. J. Smythe, B. D. Hatton, A. Grinthal, J. Aizenberg, *Nature* **2011**, 477, 443; b) D. C. Leslie, A. Waterhouse, J. B. Berthet, T. M. Valentin, A. L. Watters, A. Jain, P. Kim, B. D. Hatton, A. Nedder, K. Donovan, *Nat. Biotechnol.* **2014**, 32, 1134.
- [13] a) Y. Wang, H. Wu, Z. Zhou, M. F. Maitz, K. Liu, B. Zhang, L. Yang, R. Luo, Y. Wang, *Sci. Adv.* **2022**, 8, eabm3378; b) X. Song, H. Ji, Y. Li, Y. Xiong, L. Qiu, R. Zhong, M. Tian, J. N. Kizhakkedathu, B. Su, Q. Wei, *Nat. Biomed. Eng.* **2021**, 5, 1143; c) X. Zhao, Y. Huang, Z. Li, J. Chen, J. Luo, L. Bai, H. Huang, E. Cao, Z. Yin, Y. Han, *Adv. Mater.* **2024**, 36, 2308701; d) S. H. Jung, B. H. Jang, S. Kwon, S. J. Park, T. E. Park, J. H. Kang, *Adv. Mater.* **2023**, 35, 2211149.
- [14] S. P. Jackson, R. Darbousset, S. M. Schoenwaelder, *J. Am. Soc. Hematol.* **2019**, 133, 906.
- [15] a) J. Chen, Q. Peng, X. Peng, H. Zhang, H. Zeng, *Chem. Rev.* **2022**, 122, 14594; b) J. Zhang, L. Xiang, B. Yan, H. Zeng, *J. Am. Chem. Soc.* **2020**, 142, 1710; c) L. Xiang, J. Zhang, W. Wang, L. Gong, L. Zhang, B. Yan, H. Zeng, *Acta Biomater.* **2020**, 117, 294; d) E. Bethur, R. Guha, Z. Zhao, B. B. Katz, P. D. Ashby, H. Zeng, S. M. Copp, *ACS Nano* **2024**, 18, 3002.
- [16] Z. Zhao, M. Pan, C. Qiao, L. Xiang, X. Liu, W. Yang, X. Z. Chen, H. Zeng, *Adv. Mater.* **2023**, 35, 2208824.
- [17] H. Matsubara, T. Imai, S. Tsuji, N. Oka, Y. Egashira, Y. Enomoto, N. Nakayama, S. Nakamura, M. Shimazawa, T. Iwama, *J. Pharmacol. Sci.* **2022**, 148, 65.
- [18] a) H. Lee, S. M. Dellatore, W. M. Miller, P. B. Messersmith, *Science* **2007**, 318, 426; b) J. Wu, J. Lee, J. Y. Jung, J. H. Hwang, K. S. Kim, M. Shin, H. Lee, S. H. Park, *Adv. Mater.* **2023**, 35, 2301098; c) K. Kim, J. H. Ryu, M.-Y. Koh, S. P. Yun, S. Kim, J. P. Park, C.-W. Jung, M. S. Lee, H.-I. Seo, J. H. Kim, *Sci. Adv.* **2021**, 7, eabc9992; d) S. Hong, Y. Wang, S. Y. Park, H. Lee, *Sci. Adv.* **2018**, 4, eaat7457; e) M. A. Gebbie, W. Wei, A. M. Schrader, T. R. Cristiani, H. A. Dobbs, M. Idso, B. F. Chmelka, J. H. Waite, J. N. Israelachvili, *Nat. Chem.* **2017**, 9, 473; f) S. Kim, J. Huang, Y. Lee, S. Dutta, H. Y. Yoo, Y. M. Jung, Y. Jho, H. Zeng, D. S. Hwang, *Proc. Natl. Acad. Sci.* **2016**, 113, E847.
- [19] X. Hu, J. Tian, C. Li, H. Su, R. Qin, Y. Wang, X. Cao, P. Yang, *Adv. Mater.* **2020**, 32, 2000128.
- [20] a) P. Yang, *Macromol. Biosci.* **2012**, 12, 1053; b) D. Wang, Y. Ha, J. Gu, Q. Li, L. Zhang, P. Yang, *Adv. Mater.* **2016**, 28, 7413; c) Y. Liu, S. Miao, H. Ren, L. Tian, J. Zhao, P. Yang, *Nat. Protoc.* **2024**, 19, 539; d) C. Fu, Z. Wang, X. Zhou, B. Hu, C. Li, P. Yang, *Chem. Soc. Rev.* **2024**, 53, 1514.
- [21] H.-C. Yang, K.-J. Liao, H. Huang, Q.-Y. Wu, L.-S. Wan, Z.-K. Xu, *J. Mater. Chem. A* **2014**, 2, 10225.
- [22] T. Shui, M. Pan, A. Li, H. Fan, J. Wu, Q. Liu, H. Zeng, *Chem. Mater.* **2022**, 34, 8613.
- [23] a) C. Stani, L. Vaccari, E. Mitri, G. Birarda, *Spectrochim. Acta, Part A* **2020**, 229, 118006; b) S. Zhai, Y. Ma, Y. Chen, D. Li, J. Cao, Y. Liu, M. Cai, X. Xie, Y. Chen, X. Luo, *Polym. Chem.* **2014**, 5, 1285.

- [24] A. Majumdar, S. C. Das, T. Shripathi, R. Hippler, *Compos. Interfaces* **2012**, 19, 161.
- [25] M. Suneetha, K. M. Rao, S. S. Han, *ACS Omega* **2019**, 4, 12647.
- [26] L. C. Almeida, T. Frade, R. D. Correia, Y. Niu, G. Jin, J. P. Correia, A. S. Viana, *Sci. Rep.* **2021**, 11, 2237.
- [27] a) L. Xiang, J. Zhang, W. Wang, Z. Wei, Y. Chen, H. Zeng, *Adv. Funct. Mater.* **2023**, 33, 2301593; b) C. Zhang, L. Xiang, J. Zhang, C. Liu, Z. Wang, H. Zeng, Z.-K. Xu, *Chem. Sci.* **2022**, 13, 1698; c) W. Wang, Z. Zeng, L. Xiang, C. Liu, D. Diaz-Dussan, Z. Du, A. B. Asha, W. Yang, Y.-Y. Peng, M. Pan, R. Ravin, H. Zeng, *ACS Nano* **2021**, 15, 9913.
- [28] C. Fu, Z. Wang, Y. Gao, J. Zhao, Y. Liu, X. Zhou, R. Qin, Y. Pang, B. Hu, Y. Zhang, *Nat. Sustain.* **2023**, 6, 984.
- [29] Y. Zhong, M. Ye, L. Huang, L. Hu, F. Li, Q. Ni, J. Zhong, H. Wu, F. Xu, J. Xu, *Adv. Mater.* **2022**, 34, 2109955.
- [30] H. Geng, P. Zhang, Q. Peng, J. Cui, J. Hao, H. Zeng, *Acc. Chem. Res.* **2022**, 55, 1171.
- [31] M. Guglin, M. J. Zucker, V. M. Bazan, B. Bozkurt, A. El Banayosy, J. D. Estep, J. Gurley, K. Nelson, R. Malyala, G. S. Panjra, *J. Am. Coll. Cardiol.* **2019**, 73, 698.
- [32] a) W. Cao, W. Cao, W. Zhang, X. L. Zheng, X. F. Zhang, *J. Thromb. Haemost.* **2020**, 18, 2169; b) X. D. Manz, H. J. Bogaard, J. Aman, *Arterioscler., Thromb., Vasc. Biol.* **2022**, 42, 1307.